

Characterization of the high-affinity anti-CTLA-4 monoclonal antibody JS007 for immune checkpoint therapy of cancer

Jiawei Guan, Hongchuan Liu, Yan Chai, Jie Yu, Jian Yao, Jing Wang, Zhiwei Pan, Jing Zhang, Yuehua Zhou, Hui Liu, Sheng Yao, Jianxun Qi, Hui Feng, George F. Gao, Qihui Wang, Yi Shi & Shuguang Tan

To cite this article: Jiawei Guan, Hongchuan Liu, Yan Chai, Jie Yu, Jian Yao, Jing Wang, Zhiwei Pan, Jing Zhang, Yuehua Zhou, Hui Liu, Sheng Yao, Jianxun Qi, Hui Feng, George F. Gao, Qihui Wang, Yi Shi & Shuguang Tan (2023) Characterization of the high-affinity anti-CTLA-4 monoclonal antibody JS007 for immune checkpoint therapy of cancer, mAbs, 15:1, 2153409, DOI: [10.1080/19420862.2022.2153409](https://doi.org/10.1080/19420862.2022.2153409)

To link to this article: <https://doi.org/10.1080/19420862.2022.2153409>



© 2022 The Author(s). Published with license by Taylor & Francis Group, LLC.



[View supplementary material](#)



Published online: 13 Dec 2022.



[Submit your article to this journal](#)



Article views: 535

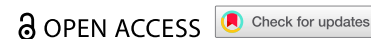


[View related articles](#)



[View Crossmark data](#)

REPORT



Characterization of the high-affinity anti-CTLA-4 monoclonal antibody JS007 for immune checkpoint therapy of cancer

Jiawei Guan^{a,b#}, Hongchuan Liu^{c#}, Yan Chai^{a#}, Jie Yu^d, Jian Yao^c, Jing Wang^c, Zhiwei Pan^c, Jing Zhang^c, Yuehua Zhou^c, Hui Liu^c, Sheng Yao^c, Jianxun Qi^a, Hui Feng^c, George F. Gao^{a,b}, Qihui Wang^{a,b}, Yi Shi^{a,b}, and Shuguang Tan^{a,b}

^aKey Laboratory of Pathogenic Microbiology and Immunology, Institute of Microbiology, Chinese Academy of Sciences (CAS), China; ^bSavaid Medical School, University of Chinese Academy of Sciences, Beijing, China; ^cDepartment of Antibody Discovery and Engineering, Shanghai Junshi Biosciences Co Ltd, Shanghai, China; ^dPilot National Laboratory for Marine Science and Technology (Qingdao), Shandong, China

ABSTRACT

Cytotoxic T lymphocyte-associated antigen 4 (CTLA-4) is a critical inhibitory checkpoint molecule, and monoclonal antibodies (mAbs) targeting CTLA-4 that restore anti-tumor T cell immunity have achieved clinical success. Here, we report a humanized IgG1 mAb, namely JS007, with high binding affinity to CTLA-4. JS007 shows superior binding affinity and T-cell activating efficiency over ipilimumab. Moreover, it demonstrates substantial *in vivo* tumor suppression efficacy at low doses. The crystal structure of JS007/CTLA-4 complex (PDB: 8HIT) shows JS007 adopts a heavy-chain-dominant binding mode, and mainly contacts the BC loop, DE loop and FG loop of CTLA-4. Notably, two Tyr residues (VH-Y100 and VL-Y32) from the complementarity-determining region loops insert into the two cavities formed by the residues from the loops of CTLA-4, which may contribute to the stabilization of the binding. Comparative analysis with other anti-CTLA-4 mAbs indicates that the double “wedge-into-hole” binding mode is unique for JS007 and may be responsible for the high-affinity binding to CTLA-4. These findings have provided an important molecular understanding of the high-affinity CTLA-4 blockade mAbs and shed light on future development of agents targeting CTLA-4.

ARTICLE HISTORY

Received 03 August 2022
Revised 24 November 2022
Accepted 26 November 2022

KEYWORDS





CTLA-4; antibody; high affinity; structure; JS007

Introduction


Immune checkpoint therapy (ICT), or immune checkpoint blockade, takes advantage of the restoration of preexisting anti-tumor T cell immunity and has reshaped the scenario of clinical therapy for tumors.^{1–3} Cytotoxic T lymphocyte-associated antigen 4 (CTLA-4), first discovered in 1987, competes the common ligands B7-1/B7-2 with stimulatory CD28 to negatively regulate T cell reactivity and serves as a critical inhibitory checkpoint molecule.⁴ Studies demonstrated that CTLA-4 is mainly expressed in regulatory T cells (Treg) and controls immune tolerance by enabling Tregs to rip B7-1/B7-2 molecules off the antigen-presenting cells.⁵ The binding of CTLA-4 can induce the endocytosis of B7-1/B7-2 molecules into CTLA-4-expressing cells, and then result in B7 degradation. Monoclonal antibodies (mAbs) that target CTLA-4 to block the interaction between CTLA-4 and its ligands have been proven to be beneficial in activating anti-tumor immunity, and been approved in clinical treatment of multiple tumors.

Currently, two CTLA-4 targeting mAbs, ipilimumab (Bristol-Myers Squibb, IgG1 subtype) and tremelimumab (AstraZeneca, IgG2 subtype) are extensively investigated in clinical trials.^{6,7} Ipilimumab became the first ICT mAb to be commercialized when it was granted an approval by the US Food and Drug Administration (FDA) in 2011.⁸ To date, tremelimumab has not been approved as monotherapy, but it

was approved by FDA in 2022 in combination with Imfinzi (anti-PD-L1 durvalumab) for hepatocellular carcinoma.⁹ Combination therapy of ipilimumab with anti-PD-1 mAbs can substantially improve survival of cancer patients and has gained particular interest in recent years.^{10–13} A large-scale Phase 3 clinical trial in patients with advanced melanoma revealed that the ipilimumab and nivolumab combination arm had a median survival of more than 60 months, whereas the ipilimumab-only arm had a median survival of 19.9 months.¹⁴ However, high rates of severe (grades 3–4) immunotherapy-related adverse effects (irAEs) were also observed with ipilimumab, which is higher than that with anti-PD-1 nivolumab (NCT03048136, NCT03048136).^{15,16} The pH-sensitive mAb HL32, which dissociates from CTLA-4 after endocytosis and allows CTLA-4 recycling, has been shown to decrease immunotherapy-related adverse effects in mouse model.^{17–19} The structures of these mAbs with CTLA-4 have been reported and the binding and blocking mechanisms defined.^{20,21} Ipilimumab and tremelimumab bind to the same region on CTLA-4 and mainly locate on the front β -sheet, which is also occupied by its ligands. The complex structure of HL32 and CTLA-4 reveals that multiple histidines are observed within the interface and may be responsible for the pH-sensitive binding, which is also observed in the structure of pH-sensitive mAbs targeting the PD-L1.²²

CONTACT Qihui Wang  wangqihui@im.ac.cn; Yi Shi  shiyi@im.ac.cn; Shuguang Tan  tansg@im.ac.cn  Key Laboratory of Pathogenic Microbiology and Immunology, Institute of Microbiology, Chinese Academy of Sciences (CAS), China

[#]These authors contributed equally

 Supplemental data for this article can be accessed online at <https://doi.org/10.1080/19420862.2022.2153409>

© 2022 The Author(s). Published with license by Taylor & Francis Group, LLC.

This is an Open Access article distributed under the terms of the Creative Commons Attribution-NonCommercial License (<http://creativecommons.org/licenses/by-nc/4.0/>), which permits unrestricted non-commercial use, distribution, and reproduction in any medium, provided the original work is properly cited.

Here, we identified a CTLA-4 specific humanized mAb JS007 with superior binding affinity and tumor suppression efficacy over ipilimumab. Structural studies of the interaction between JS007 and CTLA-4 revealed that JS007 adopts a unique “wedge-into-hole” binding mode to engage the CTLA-4, which may be responsible for the high-binding affinity. These findings will greatly enhance our understanding of high-binding affinity CTLA-4 blockade antibody and provide a structural basis for further engineering modification.

Results

Superior binding, blocking and T cell activating reactivity of JS007

By using serial dilutions of JS007 proteins to stain Chinese hamster ovary (CHO) cells stably expressing CTLA-4 (CHO-CTLA-4), a flow cytometry-based binding assay was performed to investigate the dose-dependent binding of JS007. The binding of ipilimumab was analyzed in parallel as a positive control. The results reveal that the concentration for 50% of maximal binding (EC_{50}) of JS007 (0.22 $\mu\text{g/mL}$) is about 6 times lower than that of ipilimumab (EC_{50} = 1.37 $\mu\text{g/mL}$), indicating JS007 has a higher binding affinity than that of ipilimumab (Figure 1a). The binding characteristics of JS007 and ipilimumab were further analyzed by using a protein-based surface plasmon resonance (SPR) assay (Figure 1b). JS007 proteins

were immobilized on the chip and subsequently saturated with serial dilutions of CTLA-4 proteins. Similar to the results of the flow-cytometry-based binding assay, the binding affinity of JS007 to CTLA-4 (K_D = 0.21 nM) is also substantially higher than that of ipilimumab (K_D = 16.1 nM) (supplementary Figure S1 and Table S1).

The blockade of the binding between CTLA-4 and its ligands is the key mechanism for CTLA-4-specific mAbs in reactivation of anti-tumor T cell immunity. Therefore, the blocking efficiencies of JS007 and ipilimumab were further tested in a cell-based flow cytometry assay (Figure 1c). The binding of CTLA-4 to B7-1 was analyzed by using B7-1-mFc proteins to stain CHO-CTLA-4 cells, whereas the blockade of CTLA-4/B7-1 interaction was tested with serial dilutions of JS007 or ipilimumab proteins pre-incubated with CHO-CTLA-4 cells before staining with B7-1-mFc proteins. The results demonstrated that JS007 could block the interaction between CTLA-4 and B7-1 with 50% inhibition concentration (IC_{50}) of 1.096 $\mu\text{g/mL}$, which was about 4 times lower than that of ipilimumab (IC_{50} = 4.399 $\mu\text{g/mL}$).

The T-cell activating potency of JS007 was further investigated with primary T cells. We measured the ability of JS007 to promote T cell reactivity *in vitro* by mixed leukocyte reactions (MLR) assay using allogeneic human dendritic cells (DC) and T cells. Upregulated secretion of IL-2 upon stimulation with JS007 was detected in a dose-dependent manner (Figure 1d). The fold-change of IL-2 levels in the presence of 2 $\mu\text{g/mL}$ and

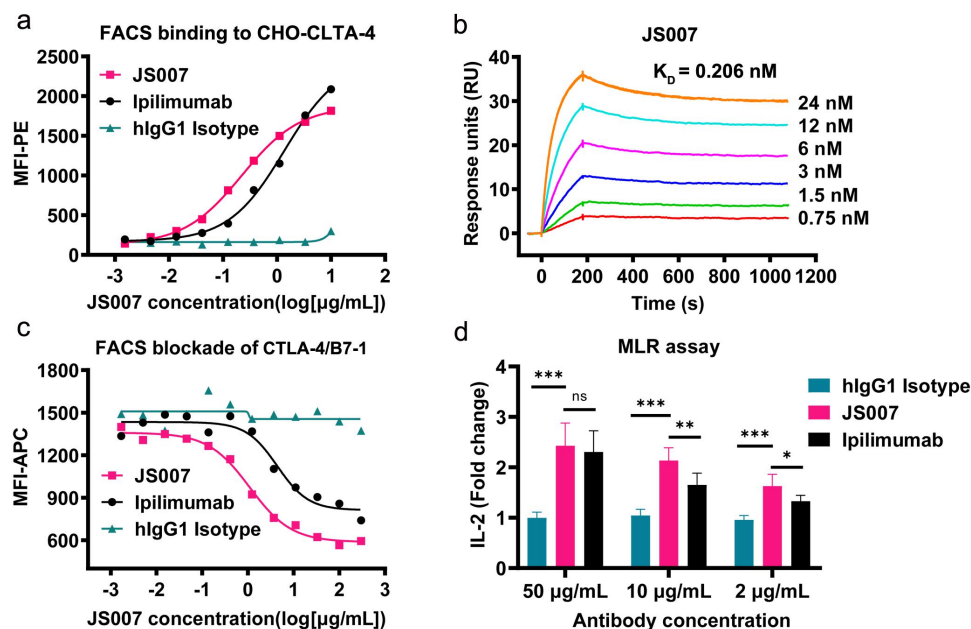


Figure 1. Binding, blocking and T cell activating characteristics of JS007. (a) Flow cytometry-based assay to test the binding between JS007 and CTLA-4, with serially diluted JS007 proteins to stain CHO cells stably expressing CTLA-4. (b) SPR analysis of the binding profiles between JS007 and CTLA-4. (c) Flow cytometry-based blocking assay to analyze the blocking of CD80-mFc protein to CHO cells stably expressing CTLA-4, with serially diluted JS007 proteins added. The binding and blocking of ipilimumab was tested in parallel as control, whereas human IgG1 isotype was analyzed as negative control. (d) Enhanced IL-2 production of T cells stimulated with allogeneic human dendritic cells in the presence of varied concentrations of JS007 as indicated. The concentration of IL-2 was measured with ELISA assay. Stimulation with serial dilutions of ipilimumab or human IgG1 isotype control were also enrolled as controls. Statistical analysis was calculated with student's T test. ***, $p < .001$; **, $p < .01$; *, $p < .05$; ns, $p > .05$.

10 $\mu\text{g/mL}$ JS007 proteins was significantly higher than that of ipilimumab ($p < .05$), whereas JS007 demonstrates comparable fold-change of IL-2 levels to ipilimumab at the high concentration of 50 $\mu\text{g/mL}$. These results indicate that JS007 engages with CTLA-4 with superior binding affinity, blocking efficiency and T cell activation potency over ipilimumab.

In vivo tumor suppression of JS007

We next investigated the *in vivo* tumor inhibition activity of JS007 in MC38 and H22 syngeneic tumor model with human CTLA-4 knock-in mice. Two groups were included, with JS007 injected at 0.1 mg/kg (low dose group) or 1 mg/kg (high dose group) via intraperitoneal injection twice a week in the MC38

tumor model. Ipilimumab and IgG1 isotype control mAbs were injected at 1 mg/kg as controls. The results showed that the tumor volume and tumor weight in the high dose group demonstrated substantial tumor suppression efficacy compared with the hIgG1 isotype control group (Figure 2 a and b). Of note, both the tumor volume and tumor weight of the JS007 high dose group were significantly lower than that of the ipilimumab group, suggesting better tumor inhibition efficacy of JS007 than ipilimumab ($p < .05$). The tumor inhibition efficacy in H22 syngeneic tumor model demonstrated a similar scenario compared to that observed in the MC38 model (Figure 2 c and d). Both tumor volume and tumor weight were substantially lower in the JS007 high dose group (0.1 mg/kg) ($p < .01$). The tumor inhibition efficacy of JS007

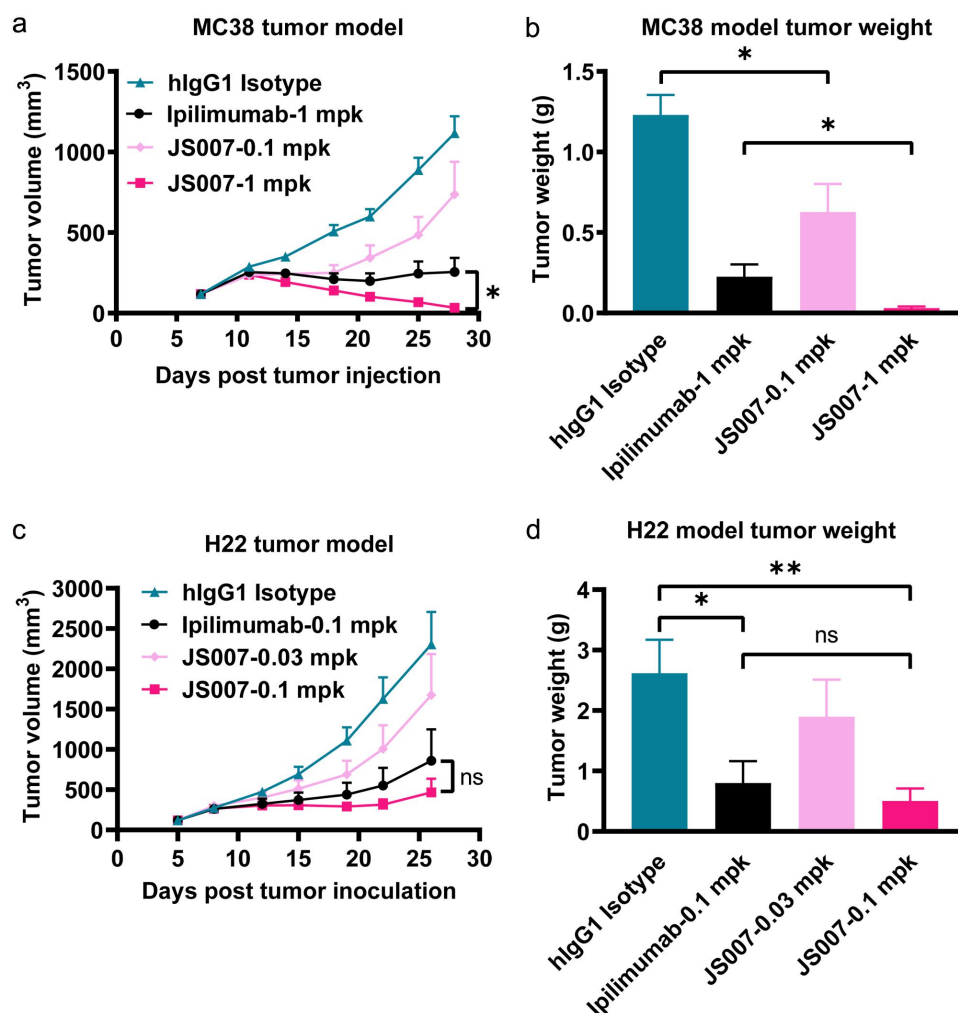


Figure 2. Tumor inhibition potency of JS007 in syngeneic tumor model. (a) The *in vivo* tumor suppression efficacy of JS007 in hCTLA-4 knock-in mice of the C57BL/6 background by inoculation of MC38 tumor cell line. JS007 was injected *i.p.* twice a week in low dose groups (0.1 mg/kg) and high dose group (1 mg/kg). 1 mg/kg of ipilimumab or hlgG1 isotype antibodies were injected as control. The data with each dot shows the average tumor volume of the group while the SE was presented as longitudinal bars. (b) The tumor weight of each group at the end of the experiment was shown. (c) The *in vivo* tumor suppression efficacy of JS007 in hCTLA-4 knock-in mice of the BALB/c background by inoculation of H22 tumor cell line. JS007 was injected *i.p.* twice a week in two groups, 0.03 mg/kg low dose group and 0.1 mg/kg high dose group. 0.1 mg/kg of ipilimumab or hlgG1 isotype antibodies were injected as control. (d) The tumor weight of each H22 syngeneic tumor group at the end of the experiment was shown. Statistical analysis was calculated with Wilcoxon paired T test. *, $p < .05$; ns, $p > .05$.

showed a better trend than that of ipilimumab in the H22 model, though no statistical significance was observed ($p > .05$).

Structural basis for the interaction between JS007 and CTLA-4

To elucidate the molecular mechanism of the binding of JS007 to CTLA-4, the structure of the CTLA-4 and JS007 complex was determined. The single-chain variable fragment (scFv) of JS007 and extracellular domain (residues 31–161) of CTLA-4 (CTLA-4-ECD) were constructed and expressed in *E. coli* cells as inclusion bodies. Soluble JS007-scFv and CTLA-4-ECD proteins were renatured through *in vitro* refolding processes with inclusion bodies. Complex proteins were obtained after co-incubation of CTLA-4-ECD and JS007-scFv proteins, and were further used for crystal screening (supplementary Figure S2). The crystal structure of CTLA-4-ECD and JS007-scFv complex was determined at a resolution of 3.2 Å (supplementary Table S2).

Overall, JS007 uses both the heavy chain (VH) and light chain (VL) to bind to CTLA-4, and buries a surface area of 833 Å² (Figure 3a). The binding interface mainly locates on the N-terminal loop, BC loop, DE loop and FG loop of CTLA-4. The three HCDR loops of JS007 form 171 atom-to-atom contacts to the residues from BC and FG loop of CTLA-4, substantially more than that formed between the LCDR loops of JS007 and the residues from N-terminal loop, BC loop and DE loop of CTLA-4 (89 atom-to-atom contacts) (supplementary Table S3). Ten hydrogen bond interactions are formed between CTLA-4 and JS007. Specifically, the HCDR3 loop of VH domain (L100, Y101, S102 and Y104) formed five hydrogen bonds with residues from BC loop (P63, K65) and FG loop (P136) of CTLA-4, indicating a dominant role of HCDR3 in the interaction with CTLA-4 (Figure 3b; supplementary Table S3). Residues from HCDR1 (Y33), HCDR2 (Y54) and VL (T31, Y53 and D92) also formed hydrogen bond interactions with residues from BC loop (E59, K65), DE loop (D110), FG loop (Y135) and G strand (Y140) (Figure 3c).

The interaction network between JS007 and CTLA-4 involves multiple aromatic residues. Of note, the ¹³⁴MYPPPY¹³⁹ loop (FG loop) of CTLA-4 dominates the interactions with HCDR1 and HCDR2, and half of the interactions with HCDR3. There are two cavities at the clefts formed by the BC loop, DE loop and FG loop (Figure 3d). Interestingly, Y100 of the HCDR3 inserts into the cavity formed by BC loop and FG loop, and forms a hydrogen bond interaction with the residue P136 in the cavity (Figure 3e), while Y32 of the LCDR1 inserts into the cavity formed by BC loop and DE loop and formed multiple Van der Waals contacts with the residues constituting the cavity. The two Tyr residues, Y100 from HCDR3 and Y32 from LCDR1, act like two wedge anchors and insert into the two cavities of CTLA-4, stabilizing the binding of JS007 with CTLA-4 (Figure 3e). Therefore, we propose that the superior binding of JS007 to CTLA-4 mainly lies on two aspects: 1) multiple aromatic residues in the CDR loops of both VH and VL domain forming complicated

interacting network with CTLA-4; and 2) the double “wedge-into-hole” binding mode with two Tyr anchoring residues from JS007 inserting into the holes on the surface of CTLA-4.

The structure of JS007-scFv/CTLA-4 complex was superimposed with that of CTLA-4/B7-1 or CTLA-4/B7-2 complex (PDB:1I8L and 1I85), respectively. The results reveal that the binding of JS007 to CTLA-4 results in steric clash to the binding of B7-1 or B7-2, and the competitive binding is mainly through the VH domain of JS007. The binding region on CTLA-4 by JS007 is overlapped with that by B7-1/B7-2 (Figure 4 a and c).^{23,24} The overlapped binding area mainly locates on the FG loop of CTLA-4 (Y135, P137, P138, Y140), which is critical for the binding of CTLA-4 to the concave surface of B7-1 or B7-2 (Figure 4 b and d). These results indicate that the blocking mechanism of JS007 relies on the VH domain, which binds to the same region on CTLA-4 recognized by B7-1 or B7-2, and thereafter interrupts the binding of ligands.

Distinct binding epitope of JS007 on CTLA-4

In addition to the structure of the JS007/CTLA-4 complex reported here, the complex structure of CTLA-4 with the other mAbs, ipilimumab (PDB:6RP8), tremelimumab (PDB:5GGV) and HL32 (PDB:6XY2), have been reported.^{19,21,25} Therefore, comparative analysis was further performed to elucidate the binding mechanisms of distinct CTLA-4-targeting mAbs (Figure 5). Overall, the binding epitope of JS007 resembles that of HL32, but is substantially distinct from that of ipilimumab and tremelimumab. We previously reported that the epitope regions of ipilimumab and tremelimumab resemble each other.^{20,21} Previous studies reported that the binding affinity between HL32 and CTLA-4 ($K_D = 199$ nM) is lower than those of the other three mAbs and substantially decreases in low pH conditions, whereas the binding of JS007 is the highest among these four mAbs. Comparative structural analysis reveals that the buried surface area by HL32 is substantially smaller than the other three mAbs. Moreover, the double “wedge-into-hole” anchor residues are not presented in HL32, and the two cavities in CTLA-4, which are inserted with two Tyr anchor residues from JS007, are not occupied in the complex structure (supplementary Figure S3). Therefore, the comparative analysis indicates that the superior binding affinity of JS007 may be predominantly due to the unique double “wedge-into-hole” binding mode.

Superposition of CTLA-4 molecules extracted from complexes with the four mAbs and its ligands revealed that the overall structures of CTLA-4 are highly conserved, but variations in the loops that connect the strands could be observed (supplementary Figure S3). The conformations of the two cavities responsible for the double “wedge-into-hole” binding of JS007 varied with the CTLA-4 molecules extracted from the other complexes, indicating that these flexible loops accommodate the anchoring residues of JS007 through fine tuning to form proper cavities.

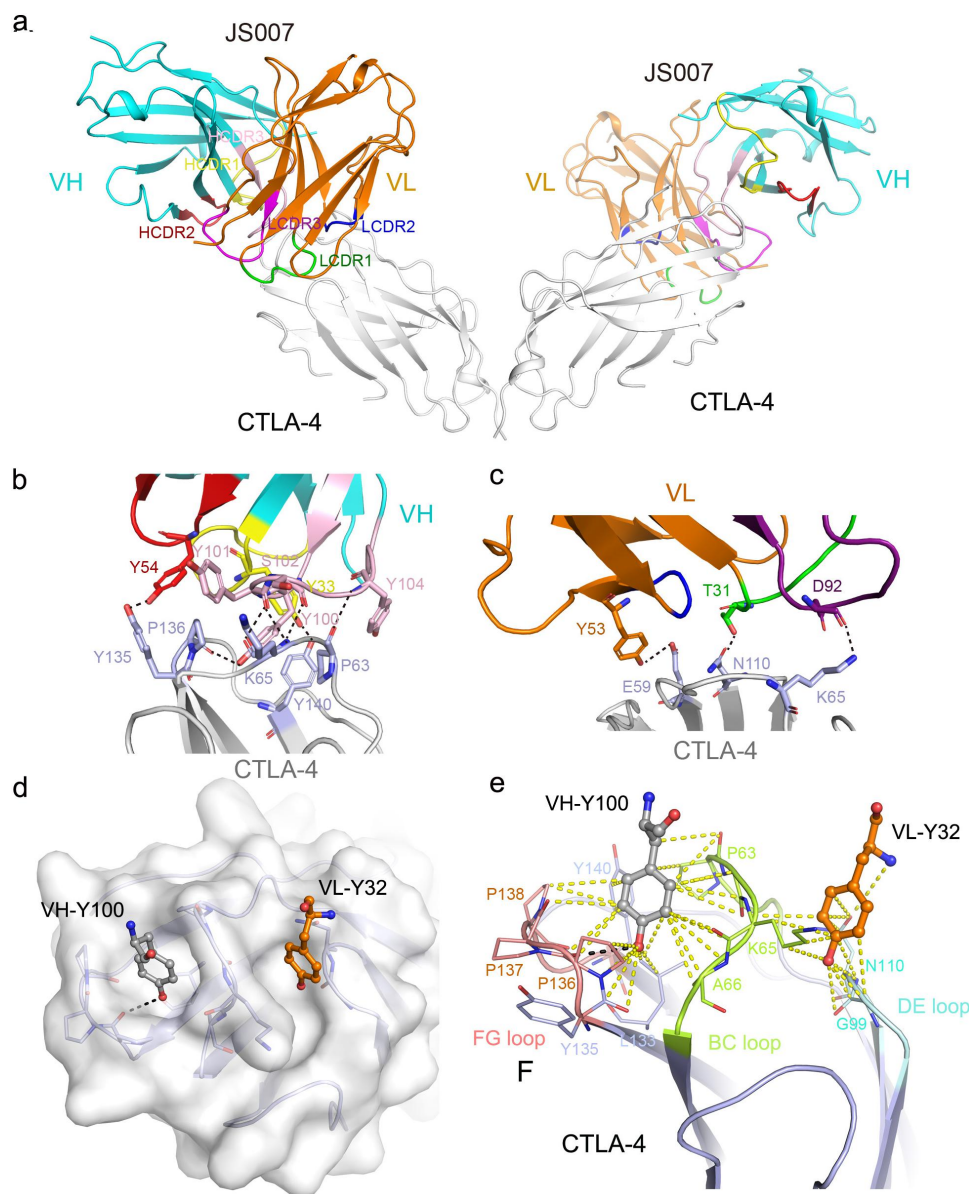


Figure 3. Structural basis for the interaction between JS007-scFv and CTLA-4. (a) Overall structure of the JS007-scFv and dimeric CTLA-4 complex. CTLA-4 is shown as cartoon representations in gray, and the heavy (VH) and light chains (VL) of scFv are shown in cyan and Orange, respectively. The CDR1, CDR2 and CDR3 loops of VH are colored in yellow, red, and light pink, respectively. The CDR1, CDR2 and CDR3 loops of VL are colored in green, blue and purple, respectively. (b-c) Detailed interactions involving the VH domain (b) and VL domain (c) of JS007 within the interface of JS007/CTLA-4 complex. The residues involved in the hydrogen bond interactions are shown as sticks and labeled. Hydrogen bonds are shown as dash lines. (d) Highlights of the two Tyr residues from JS007 inserting into the cavities on the surface of CTLA-4. The CTLA-4 is shown as electrostatic potential surface and the two Tyr residues present as sticks. (e) Detailed interactions involving the two Tyr residues with residues from the BC loop, DE loop and FG loop. Hydrogen bonds are shown as black dash lines, while Van der Waals interactions are shown as yellow dash lines.

CTLA-4 is presented as a cysteine-linked homodimer on the cell surface, and we therefore modeled the binding of the full-length mAbs to the dimeric CTLA-4 molecules (Figure 6). CTLA-4 is formed by two β sheet faces and the dimerization mainly positioned carboxy terminal region. We measured the distance to see whether a full-length antibody could bind to the two CTLA-4 molecules in the dimer. The binding of the mAbs to CTLA-4 adopt distinct orientations and the two Fabs of the antibody cannot bind simultaneously to the two CTLA-4 molecules in a dimer. On the other side, an antibody may bind to two different CTLA-4 dimers that the other binding region of the antibody is free and could adopt to bind to another CTLA-4.

Discussion

The anti-tumor effects of CTLA-4 targeting therapeutic mAbs mainly rely on two aspects: 1) inhibition of the interaction between CTLA-4 and its ligands; and 2) depletion of tumor-infiltrated Tregs with high levels of CTLA-4. The first aspect substantially depends on the superior binding affinity and competitive binding epitope that interrupts the interaction of CTLA-4 with its ligands, whereas the second aspect relies on the Fc-mediated effector function.²⁶ We demonstrate that JS007 binds to CTLA-4 with superior binding affinity over ipilimumab, which may be the causative reason for the

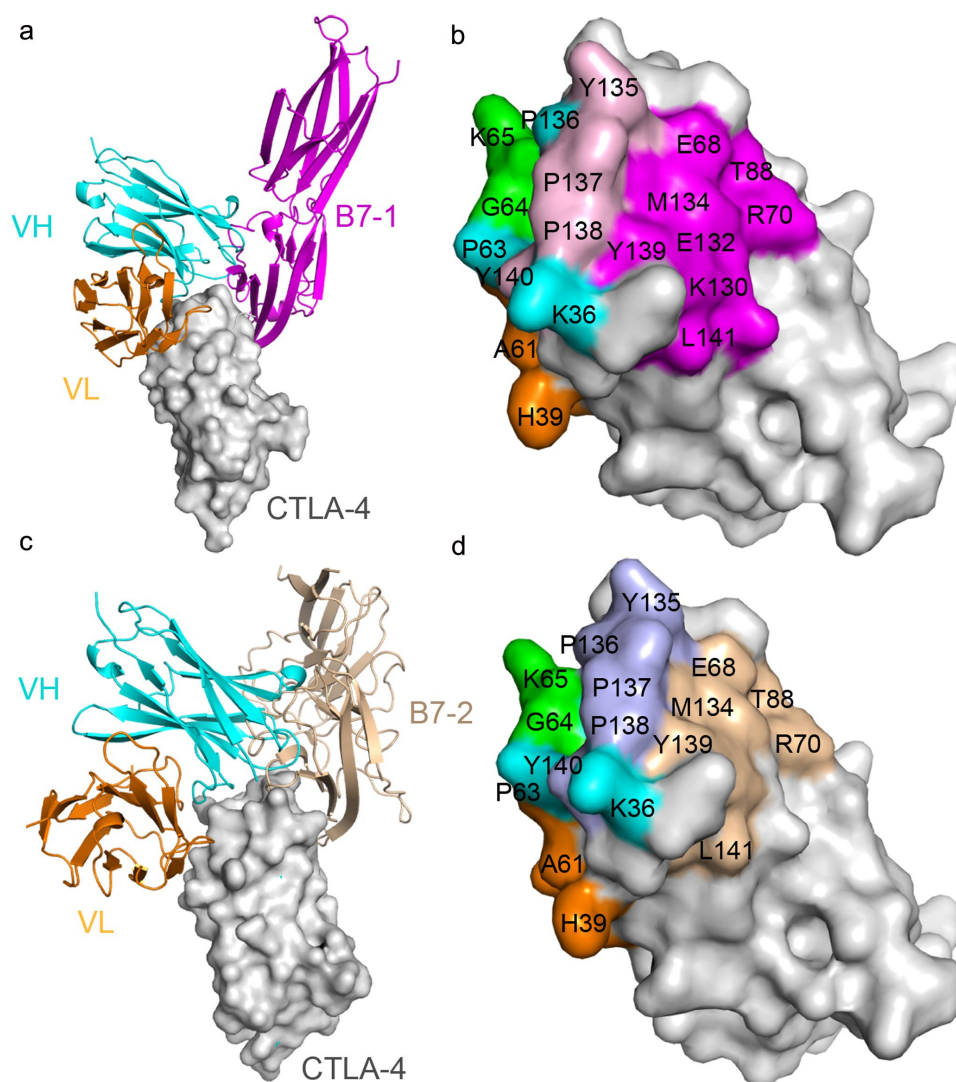


Figure 4. Competitive binding of JS007-scFv and B7-1/B7-2 with CTLA-4. (a) Superposition of the JS007/CTLA-4 complex structure with CTLA-4/B7-1 complex structure (PDB: 118L). CTLA-4 is shown as surface diagram in gray, B7-1 in pink, JS007 VH in cyan and VL in Orange, respectively. (b) Binding surface of CTLA-4 by B7-1 or JS007. The binding residues by B7-1 on CTLA-4 are colored in pink, whereas residues contacted by the JS007 VH or VL domain are colored in cyan or Orange, respectively. The residues contact with both VH and VL are colored in green, and the overlapping residues bound by both B7-1 and JS007 are colored in light pink. (c) Superposition of the JS007 /CTLA-4 complex structure with CTLA-4/B7-2 complex structure (PDB: 1185). B7-2 is shown as cartoon in brown and the other parts are the same as in (a). (d) Binding surface of CTLA-4 by B7-2 or JS007. The binding residues by B7-2 on CTLA-4 are colored in brown, whereas residues contacted by the JS007-scFv VH or VL are colored the same as in (b). The residues contact with both VH and VL are colored in green, and the overlapping residues bound by both B7-2 and JS007 are colored in light blue.

advantages of JS007, including more efficient blocking and T cell activating potency.

The binding affinity of JS007 is ~80 times higher than that of ipilimumab. Structural analysis demonstrates that the binding of JS007 to CTLA-4 mainly locates on the three loops, the BC loop, DE loop and FG loop. The interruption of the receptor/ligand interaction by JS007 is mainly due to the competitive binding to the residues from FG loop of CTLA-4, which is also the main region for the interaction with its ligands. Interestingly, two anchoring residues, Y100 from HCDR3 and Y32 from LCDR1, insert into the two cavities on the surface of CTLA-4. This double “wedge-into-hole” binding mode may help to stabilize the interaction between JS007 and CTLA-4. Moreover, the interaction network between JS007 and CTLA-4 was mainly formed by multiple aromatic residues

from the CDR loops of JS007. Therefore, we speculate that the two Tyr anchor mediated double “wedge-into-hole” binding mode and multiple aromatic residues in the CDR loops are the determinants of high affinity binding of JS007 to CTLA-4. However, the functional effects of this high affinity mAb, especially the toxicity side effects, should be further investigated.

The ¹³⁴MYPPPY¹³⁹ loop (FG loop) of CTLA-4 is found to dominate the interaction with its ligands and contributes ~80% of the interactions with B7-1 or B7-2 23–24, and binds to the concave surface presented by the front sheets of the ligands. Ipilimumab and tremelimumab, the two mAbs most widely investigated in clinical trials, bind to similar regions on the front sheet of CTLA-4, not the ¹³⁴MYPPPY¹³⁹ loop. In contrast, both JS007 and HL32 bind to the ¹³⁴MYPPPY¹³⁹ loop on

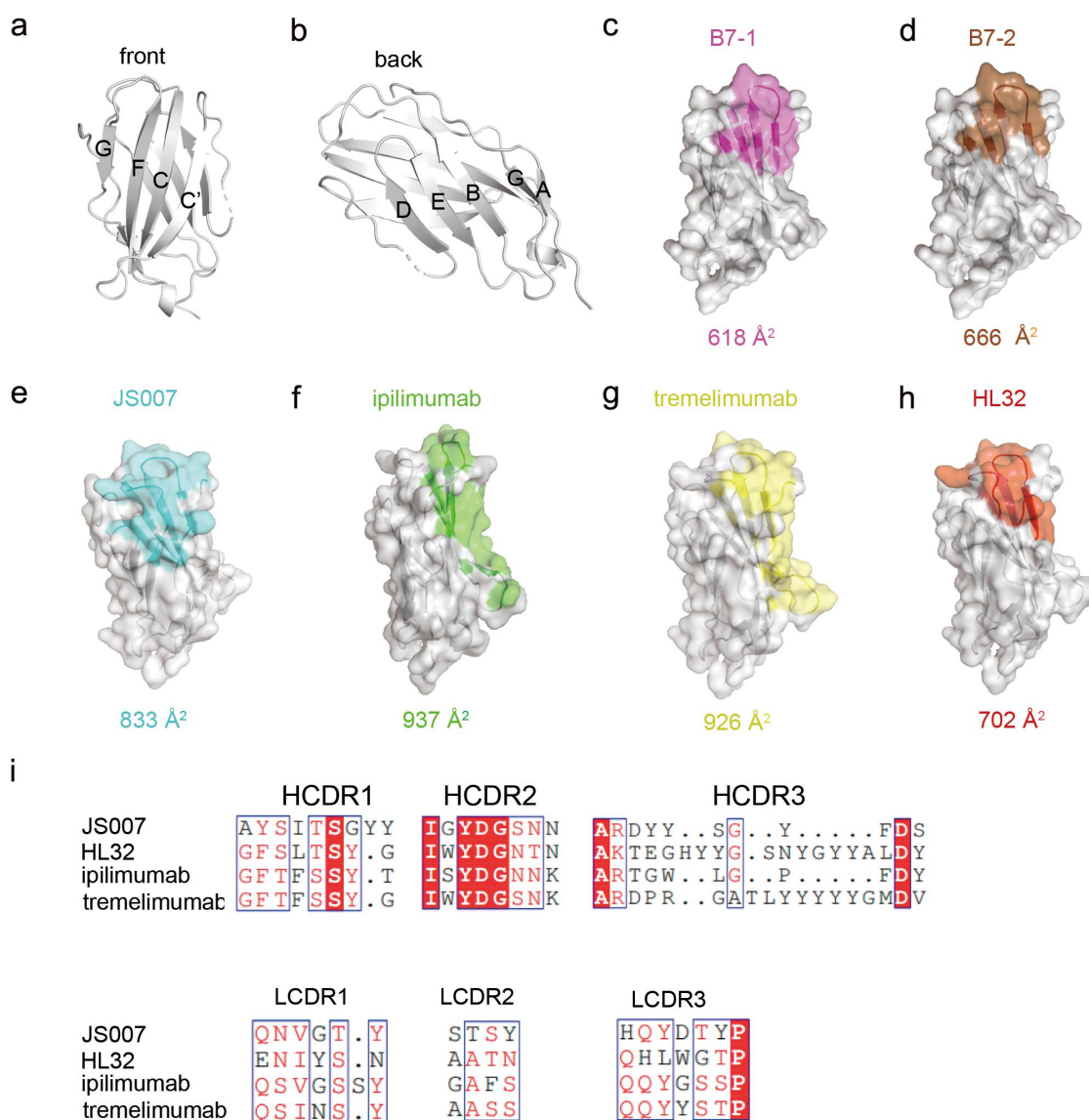


Figure 5. Comparative analysis of the binding areas of JS007, ipilimumab, tremelimumab and HL32. (a-b) The front and back of CTLA-4 is shown in cartoon. (c-h) The binding surface of B7-1, B7-2, JS007, ipilimumab, tremelimumab and HL32 on CTLA-4 were depicted and colored as indicated. The binding surface areas for the ligand or the corresponding mAbs are labeled below each surface map. (i) Sequence alignment of the CDR loops of the four mAbs.

CTLA-4 with multiple hydrogen bond interactions. The binding affinity of HL32 to CTLA-4 is comparatively lower than the other CTLA-4 mAbs, with a K_D value of 199 nM at neutral pH conditions.¹⁹ Multiple histidines involved in the interface of HL32 and CTLA-4 may be responsible for the rapid dissociation at low pH conditions.¹⁹ HL32 has an 18 aa HCDR3 loop, substantially longer than the 11 aa HCDR3 loop of JS007. The major difference of the binding affinities with CTLA-4 between these two mAbs is probably due to the double “wedge-into-hole” binding mode.

We found that the loops of CTLA-4 accommodate the two anchoring residues of JS007 through fine tuning of their conformations. The FG loop is involved in binding to the ligands, whereas the BC loop and DE loop do not engage with the ligands. The BC loop locates in the middle, while the FG loop and DE loop lie on two sides of the BC loop. The DE loop and FG loop show no substantial variations

upon binding to the ligands or mAbs, whereas the BC loop adopts varied conformations when binding to different ligands or mAbs. The variations of BC loop may preserve spaces for the insertion of anchoring residues from the mAbs. Therefore, the loops of CTLA-4 could be valuable targeting regions for future design of high affinity agents.

In conclusion, JS007 is a CTLA-4-targeting mAb with superior binding affinity and blocking efficiency, and shows substantial *in vivo* anti-tumor potency. Structure of JS007/CTLA-4 complex reveals that JS007 mainly binds to the loops of CTLA-4 with multiple aromatic residues from the CDR loops. Of note, two Tyr anchoring residues from JS007 insert into the two cavities on the surface of CTLA-4, which may be the determinant factor for the high affinity binding. These findings will contribute to an important understanding of high-affinity CTLA-4 targeting therapeutic mAbs.

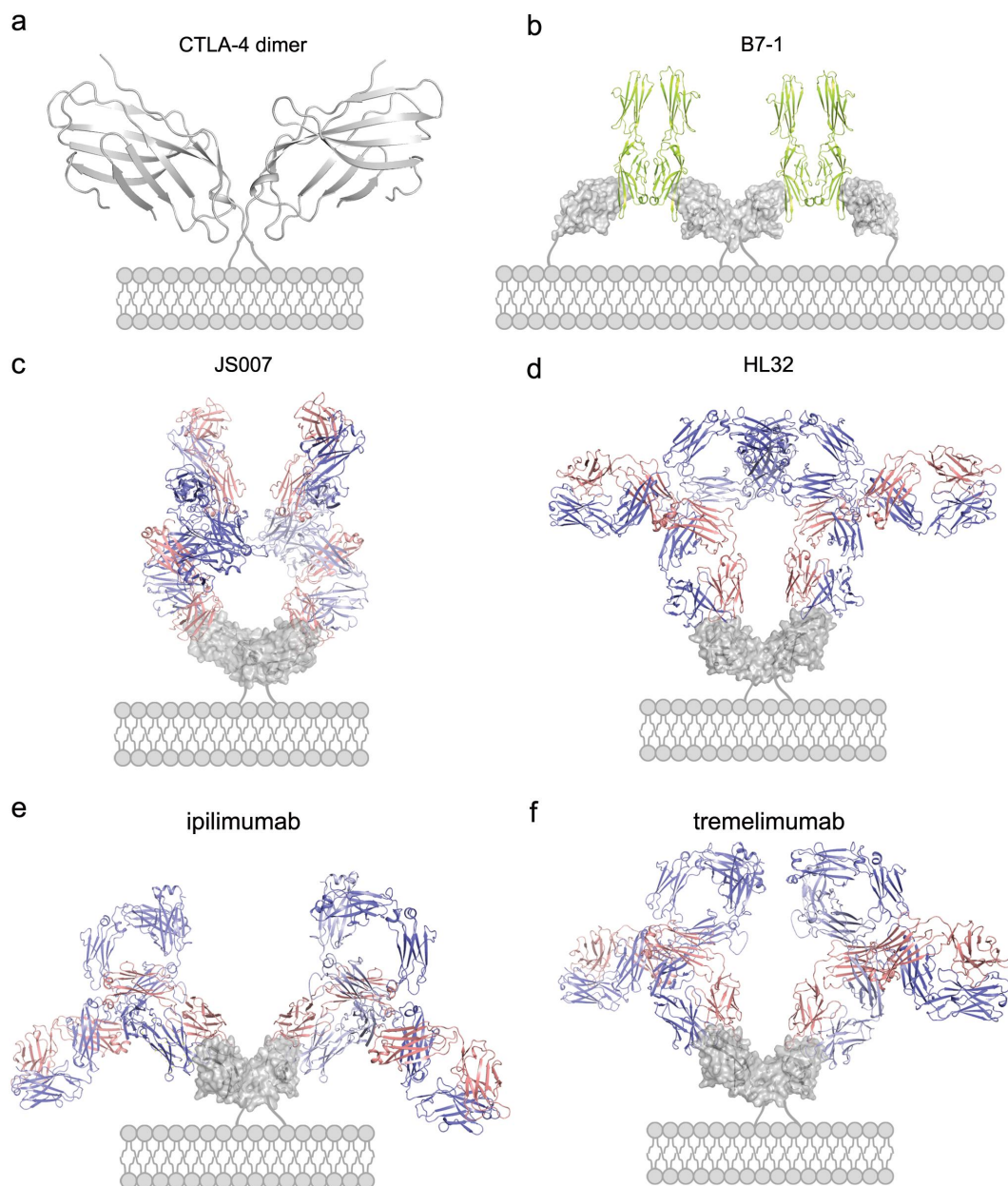


Figure 6. Structural modeling of the binding of full-length antibody to dimeric CTLA-4 on cell surface. (a-b) Structure of dimeric CTLA-4 (a) and the binding of B7-1 to dimeric CTLA-4 (b). The B7-1 is depicted in lemon while CTLA-4 in gray. (c-f) Structure of full-length JS007 (c), HL32 (d), ipilimumab (e) and tremelimumab (f) antibodies to dimeric CTLA-4. The heavy chain of antibody is presented as cartoon in blue, while the light chain is colored in salmon. The dimeric CTLA-4 is presented as surface and colored in gray.

Materials and methods

Plasmid construction and protein purification

The coding sequences for heavy chain and light chain of ipilimumab were obtained from IMGT[®], the international ImMunoGeneTics information system[®] (www.imgt.org/; INN: 8568). The heavy chain of ipilimumab and JS007 were cloned individually into HX1 vector (in-house constructed) with SapI restriction site, and the light chain were cloned individually into HX2 vector (in-house constructed) with SapI restriction site. Ipilimumab and JS007 proteins were expressed in human 293-Freestyle cells and purified by HiTrap Protein A HP column (GE Healthcare).

The DNA sequence encoding CTLA-4-ECD (31–161 AA) was subcloned as previously described.²⁰ The gene for the scFv of JS007 was constructed as VL-GG(GGSGG)3-GG-VH and subcloned into the pET21a expression vector (Invitrogen). All plasmids were transformed into *E. coli* BL21 (DE3) and the CTLA-4-ECD and JS007 scFv proteins were expressed as inclusion bodies and refolded as previously described to obtain soluble proteins.²⁰ Inclusion bodies were collected at 4°C by 12,000 rpm/min for 20 min and solubilized in dissolution buffer (50 mM Tris, 100 mM NaCl, 10 mM EDTA, 6 M guanidine hydrochloride (Gua HCl), 10 mM dithiothreitol (DTT), 10% glycerol, pH 8.0) by stirring overnight. After centrifuging (12,000 rpm/min for 10 min at 4°C) to remove undissolved protein, the solubilized proteins were

diluted into refolding buffer (100 mM Tris, 400 mM L-Arginine-HCl, 2 mM EDTA, 5 mM GSH, 0.5 mM GSSG, pH 8.0) by stirring for 4–6 h in three times. Subsequently, refolded protein was concentrated and buffer exchanged into 20 mM Tris-HCl and 150 mM NaCl, pH 8, by Amicon ultrafiltration (Millipore) with a 10,000 Da molecular mass cut off membrane. The proteins were purified and analyzed in an ÄKTA Pure (GE Healthcare Life Sciences) by gel filtration chromatography using a HiLoad 16/600 Superdex™ 200pg column (GE Healthcare Life Sciences). The protein qualities were evaluated by reduced and nonreduced 15% SDS–PAGE gel and stained with Coomassie blue. The JS007-scFv/CTLA-4 complex was formed by incubating CTLA-4 and JS007-scFv in 1:2.5 molar ratio at 4°C for 0.5 h. In a similar manner, the complex of JS007-scFv/CTLA-4 was purified and analyzed by using HiLoad 16/600 Superdex™ 200pg column (GE Healthcare Life Sciences) and 15% SDS–PAGE gel stained with Coomassie blue.

SPR analysis

The determination of the binding characteristics of JS007 and ipilimumab toward human CTLA-4 was performed on Biacore T200 system with series S sensor chip CM5 (GE Healthcare, Catalog No. BR100530) at 25°C. For surface preparation, 40 µg/mL goat anti-human IgG Fc antibodies (Jackson ImmunoResearch, Catalog No. 109–001–008) was immobilized on both flow cells of CM5 sensor chip, and then 0.5 µg/mL JS007 or ipilimumab was injected into flow cells, with the first flow cell as the reference channel, the second flow cell as the test channel. For JS007 binding characterization, serially diluted recombinant human CTLA-4-His-tag proteins (0.75 nM, 1.5 nM, 3 nM, 6 nM, 12 nM and 24 nM) were then injected through both channels. For ipilimumab binding characterization, serially diluted recombinant human CTLA-4-His-tag proteins (7.5 nM, 15 nM, 30 nM, 60 nM, 120 nM and 240 nM) were then injected through both channels. For each cycle, after antigen association and dissociation, the sensor surface was regenerated with 10 mM glycine-HCl (pH 1.5). Kinetic binding data were analyzed with Biacore T200 Evaluation Software (Version 3.0) using 1:1 binding model.

Flow cytometry-based blocking assays

In the flow cytometry-based blocking assay, 1 µg/mL B7-1-mFc proteins were incubated with CHO-hCTLA-4 cells, together with a titration of JS007 and ipilimumab antibody (a threefold dilution series from starting concentration 300 µg/mL and a blank control). Cell surface bound B7-1-mFc proteins were subsequently detected by incubation with allophycocyanin-labeled goat anti-mouse IgG secondary antibody (Abcam, Catalog No. ab130782). Half-maximal inhibitory concentrations (IC₅₀) were determined using a log (inhibitor) vs. response – variable slope curve fit (GraphPad Prism).

Stimulation of T cell reactivity with mixed leukocyte reaction assay

A MLR assay was performed to evaluate T cell reactivation activity of JS007 and ipilimumab antibodies. CD4⁺ T cells were isolated from peripheral blood mononuclear cells (PBMCs)

(AllCells) using EasySep human CD4⁺ T cells enrichment kit (StemCell Technologies, Catalog No. 19052). DCs were generated by incubating PBMCs (AllCells) first with IL-4 (1000 U/mL) and GM-CSF (1000 U/mL), followed by maturation in media containing tumor necrosis factor (1000 U/mL), IL-1β (5 ng/mL), IL-6 (10 ng/mL), and prostaglandin E2 (1 µM) for 2 days. 1×10^4 DCs and 1×10^5 CD4⁺ T cells were seeded in RPMI 1640 medium (Gibco, Catalog No. 11875093) in a 96-well plate and incubated with serial fivefold dilutions of JS007 antibody, ipilimumab analogue or control hIgG1 antibody from a starting concentration of 50 µg/mL overnight. The concentration of IL-2 in culture supernatants was measured by human IL2 HTRF kits (Cisbio, Catalog No. 62HIL02PEG) 3 days later with two duplicated wells for each sample.

In vivo anti-tumor activity in a syngeneic tumor model

The animal experiments were performed in accordance with regulations for care and use of laboratory animals at Immune Technology Corp, and were approved by Immune Technology's Institutional Animal Care and Use Committee. For both syngeneic models, the genetically modified mouse strain with human CTLA-4 knocked-in was used. All mice were kept in specific pathogen-free conditions.

In the MC38 syngeneic tumor model, human CTLA-4 knock-in mice were purchased from Jiangsu Biocytogen Co., Ltd (strain: C57BL/6-CTLA4^{tm1(CTLA4)}/Bcgen). Eight mice were enrolled in each group in MC38 model and 7 mice were included for each group in H22 model. Mice were subcutaneously inoculated with 1×10^6 MC38 cells in 100 µL phosphate-buffered saline on day 0. On day 7, the inoculated mice were randomized into four groups (tumor volume averages ~120 mm³) and treated with JS007 at 0.1 and 1 mg/kg via intraperitoneal injection twice a week. In the H22 syngeneic tumor model, human CTLA-4 knock-in mice were purchased from Shanghai Model Organisms Center, Inc. (strain: BALB/c-CTLA4^{em1(hCTLA4)Smoc}). Mice were subcutaneously inoculated with 1×10^6 H22 cells in 100 µL phosphate-buffered saline on day 0. On day 5, the inoculated mice were randomized into four groups (tumor volume averages ~100 mm³) and treated with JS007 at 0.03 and 0.1 mg/kg via intraperitoneal injection twice a week. The tumor growth was monitored twice a week and the volume of the tumors was calculated by the formula: $\frac{1}{2}$ length \times width.²

Crystal screening, data collection and structural determination

The complex of JS007-scFv/CTLA-4 was concentrated to 10 mg/mL for crystallization. Diffraction quality crystals of the complex of JS007-scFv/CTLA-4 was obtained by sitting drop vapor diffusion at 18°C by mixing 1 µL of protein with 1 µL of reservoir solution. Crystals of JS007-scFv/CTLA-4 complex grew in 100 mM Tris pH:8.5 30% w/v PEG 4000. For the purpose of protecting crystals, they were stored in the anti-freezing solution (the mixture of 2.5 µL crystallization buffer and 1 µL 20% (v/v) glycerol) before flash-cooling in liquid nitrogen. Diffraction data were collected at Shanghai Synchrotron Radiation Facility (SSRF) BL17U. All

the datasets were processed with HKL2000 software.²⁷ The structures of JS007-scFv and CTLA-4 were determined by the molecular replacement method using Phaser with previously reported antibody (PDB: 5XJ3) and CTLA-4 protein structure (PDB: 1I8L) as the search model.^{20,23,28} The atomic models were completed with Coot and refined with Phenix.^{29,30} The stereochemical qualities of the final model were assessed with MolProbity.³¹ All structure figures were prepared with Pymol (<http://www.pymol.org>). Coordinates and structure factor of the structure reported here have been deposited into the Protein Data Bank with PDB Code: 8HIT.

Abbreviations

CTLA-4: Cytotoxic T lymphocyte-associated antigen 4; mAb: monoclonal antibody; ICT: immune checkpoint therapy; Treg: regulatory T cells; DC: dendritic cells; irAEs: immunotherapy-related adverse effects; EC₅₀: 50% of maximal binding; CHO: Chinese hamster ovary; SPR: surface plasmon resonance; IC₅₀: 50% inhibition concentration; MLR: mixed leukocyte reactions; PBMC: peripheral blood mononuclear cells; scFv: single-chain variable fragment; VH: heavy chain variable domain; VL: light chain variable domain

Acknowledgments

We thank the staff of BL17U and BL19U beamline at the Shanghai Synchrotron Radiation Facility for assistance with data collection.

Disclosure statement

The authors declare no competing interests. JS007 mAb is a product from Shanghai Junshi Bioscience Co., Ltd. and is undergoing Phase 1a clinical trial in China. Shanghai Junshi Bioscience Co., Ltd. is the patent holder for JS007 (WO2022017428A1).

Funding

This work was supported by the National Key Research and Development Program of China (2021YFC2301400 and 2022YFC2302900), National Natural Science Foundation of China (NSFC, 92169208, 32222031 and 32100752).

ORCID

Shuguang Tan  <http://orcid.org/0000-0002-2599-4959>

References

- Sharma P, Allison JP. The future of immune checkpoint therapy. *Science*. 2015;348(6230):56–61. doi:10.1126/science.aaa8172. PMID: 25838373
- Tan S, Gao GF. New hope for cancer treatment: cancer immunotherapy. *Chin Sci Bull*. 2015;60:3155–57. In Chinese.
- Tan S, Chen D, Liu K, He M, Song H, Shi Y, Liu J, Zhang CW, Qi J, Yan J, et al. Crystal clear: visualizing the intervention mechanism of the PD-1/PD-L1 interaction by two cancer therapeutic monoclonal antibodies. *Protein Cell*. 2016;7(12):866–77. PMID: 27815822. doi:10.1007/s12338-016-0337-7.
- Greenfield EA, Nguyen KA, Kuchroo VK. CD28/B7 costimulation: a review. *Crit Rev Immunol*. 1998;18(5):389–418. doi:10.1615/critimmunol.v18.i5.10. PMID: 9784967
- Qureshi OS, Zheng Y, Nakamura K, Attridge K, Manzotti C, Schmidt EM, Baker J, Jeffery LE, Kaur S, Briggs Z, et al. Trans- endocytosis of CD80 and CD86: a molecular basis for the cell-extrinsic function of CTLA-4. *Science*. 2011;332(6029):600–03. PMID: 21474713. doi:10.1126/science.1202947.
- Hodi FS, O'Day SJ, McDermott DF, Weber RW, Sosman JA, Haanen JB, Gonzalez R, Robert C, Schadendorf D, Hassel JC, et al. Improved survival with ipilimumab in patients with metastatic melanoma. *N Engl J Med*. 2010;363(8):711–23. PMID: 20525992. doi:10.1056/NEJMoa1003466.
- Calabrò L, Morra A, Fonsatti E, Cutaia O, Fazio C, Annesi D, Lenoci M, Amato G, Danielli R, Altomonte M, et al. Efficacy and safety of an intensified schedule of tremelimumab for chemotherapy-resistant malignant mesothelioma: an open-label, single-arm, phase 2 study. *Lancet Respir Med*. 2015;3(4):301–09. PMID: 25819643. doi:10.1016/S2213-2600(15)00092-2.
- Nyakas M, Aamdal E, Jacobsen KD, Guren TK, Aamdal S, Hagene KT, Brunsvig P, Yndestad A, Halvorsen B, Tasken KA, et al. Prognostic biomarkers for immunotherapy with ipilimumab in metastatic melanoma. *Clin Exp Immunol*. 2019;197(1):74–82. PMID: 30821848. doi:10.1111/cei.13283.
- Calabrò L, Rossi G, Morra A, Rosati C, Cutaia O, Daffinà MG, Altomonte M, Di Giacomo AM, Casula M, Fazio C, et al. Tremelimumab plus durvalumab retreatment and 4-year outcomes in patients with mesothelioma: a follow-up of the open label, non-randomised, phase 2 NIBIT-MESO-1 study. *Lancet Respir Med*. 2021;9(9):969–76. PMID: 33844995. doi:10.1016/S2213-2600(21)00043-6.
- Larkin J, Chiarion-Sileni V, Gonzalez R, Grob JJ, Cowey CL, Lao CD, Schadendorf D, Dummer R, Smylie M, Rutkowski P, et al. Combined nivolumab and ipilimumab or monotherapy in untreated Melanoma. *N Engl J Med*. 2015;373(1):23–34. PMID: 26027431. doi:10.1056/NEJMoa1504030.
- Das R, Verma R, Sznol M, Boddupalli CS, Gettinger SN, Kluger H, Callahan M, Wolchok JD, Halaban R, Rhodapkar MV, et al. Combination therapy with anti-CTLA-4 and anti-PD-1 leads to distinct immunologic changes in vivo. *J Immunol*. 2015;194(3):950–59. PMID: 25539810. doi:10.4049/jimmunol.1401686.
- Wolchok JD, Kluger H, Callahan MK, Postow MA, Rizvi NA, Lesokhin AM, Segal NH, Ariyan CE, Gordon RA, Reed K, et al. Nivolumab plus ipilimumab in advanced melanoma. *N Engl J Med*. 2013;369(2):122–33. PMID: 23724867. doi:10.1056/NEJMoa1302369.
- Robert C, Schachter J, Long GV, Arance A, Grob JJ, Mortier L, Daud A, Carlino MS, McNeil C, Lotem M, et al. Pembrolizumab versus ipilimumab in advanced melanoma. *N Engl J Med*. 2015;372(26):2521–32. PMID: 25891173. doi:10.1056/NEJMoa1503093.
- Larkin J, Chiarion-Sileni V, Gonzalez R, Grob JJ, Rutkowski P, Lao CD, Cowey CL, Schadendorf D, Wagstaff J, Dummer R, et al. Five-year survival with combined nivolumab and ipilimumab in advanced melanoma. *N Engl J Med*. 2019;381(16):1535–46. PMID: 31562797. doi:10.1056/NEJMoa1910836.
- Du X, Liu M, Su J, Zhang P, Tang F, Ye P, Devenport M, Wang X, Zhang Y, Liu Y, et al. Uncoupling therapeutic from immunotherapy-related adverse effects for safer and effective anti-CTLA-4 antibodies in CTLA4 humanized mice. *Cell Res*. 2018;28(4):433–47. PMID: 29463898. doi:10.1038/s41422-018-0012-z.
- Hellmann MD, Paz-Ares L, Bernabe Caro R, Zurawski B, Kim SW, Carcereny Costa E, Park K, Alexandru A, Lupinacci L, de la Mora Jimenez E, et al. Nivolumab plus ipilimumab in advanced non-small-cell lung cancer. *N Engl J Med*. 2019;381(21):2020–31. PMID: 31562796. doi:10.1056/NEJMoa1910231.
- Du X, Tang F, Liu M, Su J, Zhang Y, Wu W, Devenport M, Lazarski CA, Zhang P, Wang X, et al. A reappraisal of CTLA-4 checkpoint blockade in cancer immunotherapy. *Cell Res*. 2018;28(4):416–32. PMID: 29472691. doi:10.1038/s41422-018-0011-0.
- Zhang Y, Du X, Liu M, Tang F, Zhang P, Ai C, Fields JK, Sundberg EJ, Latinovic OS, Devenport M, et al. Hijacking antibody-induced CTLA-4 lysosomal degradation for safer and more effective cancer immunotherapy. *Cell Res*. 2019;29(8):609–27. PMID: 31267017. doi:10.1038/s41422-019-0184-1.
- Gao H, Cai H, Liu J, Wang X, Zheng P, Devenport M, Xu T, Dou F, Liu Y, Zhou A. Structure of CTLA-4 complexed with a

- pH-sensitive cancer immunotherapeutic antibody. *Cell Discov.* **2020**;6(1):79. doi:[10.1038/s41421-020-00202-9](https://doi.org/10.1038/s41421-020-00202-9). PMID: 33298884
20. He M, Chai Y, Qi J, Zhang CWH, Tong Z, Shi Y, Yan J, Tan S, Gao GF. Remarkably similar CTLA-4 binding properties of therapeutic ipilimumab and tremelimumab antibodies. *Oncotarget.* **2017**;8(40):67129–39. doi:[10.18632/oncotarget.18004](https://doi.org/10.18632/oncotarget.18004). PMID: 28978021
 21. Lee JY, Lee HT, Shin W, Chae J, Choi J, Kim SH, Lim H, Won Heo T, Park KY, Lee YJ, et al. Structural basis of checkpoint blockade by monoclonal antibodies in cancer immunotherapy. *Nat Commun.* **2016**;7(1):13354. PMID: 27796306. doi:[10.1038/ncomms13354](https://doi.org/10.1038/ncomms13354).
 22. Liu H, Bi X, Zhou Y, Shi R, Yao S, Qi J, Feng H, Feng M, Yan J, Tan S. Identification of a hotspot on PD-L1 for pH-dependent binding by monoclonal antibodies for tumor therapy. *Signal Transduct Target Ther.* **2020**;5(1):158. doi:[10.1038/s41392-020-00254-z](https://doi.org/10.1038/s41392-020-00254-z). PMID: 32839442
 23. Stamper CC, Zhang Y, Tobin JF, Erbe DV, Ikemizu S, Davis SJ, Stahl ML, Seehra J, Somers WS, Mosyak L. Crystal structure of the B7-1/CTLA-4 complex that inhibits human immune responses. *Nature.* **2001**;410(6828):608–11. doi:[10.1038/35069118](https://doi.org/10.1038/35069118). PMID: 11279502
 24. Schwartz JC, Zhang X, Fedorov AA, Nathenson SG, Almo SC. Structural basis for co-stimulation by the human CTLA-4/B7-2 complex. *Nature.* **2001**;410(6828):604–08. doi:[10.1038/35069112](https://doi.org/10.1038/35069112). PMID: 11279501
 25. Ramagopal UA, Liu W, Garrett-Thomson SC, Bonanno JB, Yan Q, Srinivasan M, Wong SC, Bell A, Mankikar S, Rangan VS, et al. Structural basis for cancer immunotherapy by the first-in-class checkpoint inhibitor ipilimumab. *Proc Natl Acad Sci U S A.* **2017**;114(21):E4223–E4232. PMID: 28484017. doi:[10.1073/pnas.1617941114](https://doi.org/10.1073/pnas.1617941114).
 26. Arce Vargas F, Furness AJS, Litchfield K, Joshi K, Rosenthal R, Ghorani E, Solomon I, Lesko MH, Ruef N, Roddie C, et al. Fc effector function contributes to the activity of human anti-ctla-4 antibodies. *Cancer Cell.* **2018**;33(4):649–663.e4. PMID: 29576375. doi:[10.1016/j.ccell.2018.02.010](https://doi.org/10.1016/j.ccell.2018.02.010).
 27. Otwinowski Z, Minor W. Processing of X-ray diffraction data collected in oscillation mode. *Methods Enzymol.* **1997**;276:307–26.
 28. Read RJ. Pushing the boundaries of molecular replacement with maximum likelihood. *Acta Crystallogr D Biol Crystallogr.* **1997**;276:307–26. PMID: 27754618. doi:[10.1016/S0076-6879\(97\)76066-X](https://doi.org/10.1016/S0076-6879(97)76066-X).
 29. Emsley P, Cowtan K. Coot: model-building tools for molecular graphics. *Acta Crystallogr D Biol Crystallogr.* **2004**; 60:2126–32. doi: [10.1107/S0907444904019158](https://doi.org/10.1107/S0907444904019158). PMID: 15572765. 12
 30. Adams PD, Afonine PV, Bunkóczi G, Chen VB, Davis IW, Echols N, Headd JJ, Hung LW, Kapral GJ, Grosse-Kunstleve RW, et al. PHENIX: a comprehensive Python-based system for macromolecular structure solution. *Acta Crystallogr D Biol Crystallogr.* **2010**;66(2):213–21. PMID: 20124702. doi:[10.1107/S0907444909052925](https://doi.org/10.1107/S0907444909052925).
 31. Chen VB, Arendall WB 3rd, Headd JJ, Keedy DA, Immormino RM, Kapral GJ, Murray LW, Richardson JS, Richardson DC. MolProbity: all-atom structure validation for macromolecular crystallography. *Acta Crystallogr D Biol Crystallogr.* **2010**;66(Pt 1):12–21. doi:[10.1107/S0907444909042073](https://doi.org/10.1107/S0907444909042073). PMID: 20057044